REPORT DOCUMENTATION PAGE

Form Approved OMB NO. 0704-0188

1. REPORT DATE (DD-MM-YYYY)	2. REPORT TYPE	3. DATES COVERED (From - To)
	New Reprint	-

4. TITLE AND SUBTITLE
Metamorphic InAsSb-based barrier photodetectors for the long wave infrared region

5a. CONTRACT NUMBER
W911NF-11-1-0109

5b. GRANT NUMBER

5c. PROGRAM ELEMENT NUMBER
611102

6. AUTHORS
Leon Shterengas, Gregory Belenky, Wendy Sarney, Stefan Svensson, Ding Wang, Dmitry Donetsky, Gela Kipshidze, Youxi Lin

5d. PROJECT NUMBER

5e. TASK NUMBER

5f. WORK UNIT NUMBER

7. PERFORMING ORGANIZATION NAMES AND ADDRESSES
Research Foundation of SUNY at Stony Brook U
Office of Sponsored Programs
W-5510 Melville Library
Stony Brook, NY 11794 -3362

8. PERFORMING ORGANIZATION REPORT NUMBER

9. SPONSORING/MONITORING AGENCY NAME(S) AND ADDRESS(ES)
U.S. Army Research Office
P.O. Box 12211
Research Triangle Park, NC 27709-2211

10. SPONSOR/MONITOR'S ACRONYM(S)
ARO

11. SPONSOR/MONITOR'S REPORT NUMBER(S)
57965-EL.5

12. DISTRIBUTION AVAILIBILITY STATEMENT
Approved for public release; distribution is unlimited.

13. SUPPLEMENTARY NOTES
The views, opinions and/or findings contained in this report are those of the author(s) and should not contrued as an official Department of the Army position, policy or decision, unless so designated by other documentation.

14. ABSTRACT
InAs0.6Sb0.4/Al0.75In0.25Sb-based barrier photodetectors were grown metamorphically on compositionally graded Ga1?xInxSb buffer layers and GaSb substrates by molecular beam epitaxy. At the wavelength of 8??m and T?=?150?K, devices with 1-?m thick absorbers demonstrated an external quantum efficiency of 18% under a bias voltage of 0.45?V.

15. SUBJECT TERMS
aluminium compounds, buffer layers, gallium compounds, III-V semiconductors, indium compounds, infrared detectors, molecular beam epitaxial growth, photodetectors

16. SECURITY CLASSIFICATION OF:			17. LIMITATION OF ABSTRACT	15. NUMBER OF PAGES	19a. NAME OF RESPONSIBLE PERSON
a. REPORT	b. ABSTRACT	c. THIS PAGE			Gregory Belenky
UU	UU	UU	UU		19b. TELEPHONE NUMBER: 631-632-8397

Report Title

Metamorphic InAsSb-based barrier photodetectors for the long wave infrared region

ABSTRACT

InAs0.6Sb0.4/Al0.75In0.25Sb-based barrier photodetectors were grown metamorphically on compositionally graded Ga1?xInxSb buffer layers and GaSb substrates by molecular beam epitaxy. At the wavelength of 8??m and T?=?150? K, devices with 1-?m thick absorbers demonstrated an external quantum efficiency of 18% under a bias voltage of 0.45?V.

REPORT DOCUMENTATION PAGE (SF298)
(Continuation Sheet)

Continuation for Block 13

ARO Report Number 57965.5-EL
Metamorphic InAsSb-based barrier photodetecto ...

Block 13: Supplementary Note

Approved for public release; distribution is unlimited.

Metamorphic InAsSb-based barrier photodetectors for the long wave infrared region

Ding Wang,[1] Dmitry Donetsky,[1] Gela Kipshidze,[1] Youxi Lin,[1] Leon Shterengas,[1] Gregory Belenky,[1,a)] Wendy Sarney,[2] and Stefan Svensson[2]
[1]*Department of ECE, Stony Brook University, Stony Brook, New York 11794, USA*
[2]*U.S. Army Research Laboratory, 2800 Powder Mill Rd., Adelphi, Maryland 20783, USA*

(Received 25 June 2013; accepted 23 July 2013; published online 2 August 2013)

$InAs_{0.6}Sb_{0.4}/Al_{0.75}In_{0.25}Sb$-based barrier photodetectors were grown metamorphically on compositionally graded $Ga_{1-x}In_xSb$ buffer layers and GaSb substrates by molecular beam epitaxy. At the wavelength of 8 μm and T = 150 K, devices with 1-μm thick absorbers demonstrated an external quantum efficiency of 18% under a bias voltage of 0.45 V. © *2013 AIP Publishing LLC*. [http://dx.doi.org/10.1063/1.4817823]

Efficient photodetectors for the spectral range from 8 to 14 μm are required for a variety of applications. In the quest for the most efficient technological solution, photodetector heterostructures based on the III–V family of semiconductors have attracted significant attention for a long period of time. Barrier photodetector designs were recently developed to enhance device performance.[1–6] The generic design targets of the barrier photodetector include (a) the development of high quality narrow bandgap absorbers with sharp absorption edge and sufficiently high diffusion lengths and (b) the development of wide bandgap barrier materials with proper band alignment with respect to the absorber section. Although a large range of band gaps and band alignments are available within the III–V materials system, the requirement of high quality growth on commercially available substrates limits the practical design flexibility.

Recently, it was shown that for InAsSb-based materials utilization of compositionally graded (Al)GaInSb buffer layers can turn the lattice constant into a design parameter. This technology allowed the growth of high quality unstrained unrelaxed InAsSb bulk layers with thickness up to 4 μm on commercially available GaSb substrates.[7–11] The lattice mismatch of more than 2% between the GaSb substrate and InAsSb alloys having Sb compositions exceeding 40% is effectively accommodated by a network of misfit dislocations confined in the compositionally graded GaInSb buffer layer. It was shown that Te-doped GaInSb relaxed layers do not impede electron transport and thus do not cause any significant voltage penalty in light emitting and laser diodes.[8–10] Transmission electron microscopy (TEM) studies demonstrated that the density of dislocations threading into the bulk unstrained unrelaxed InAsSb from the GaInSb buffers is below the limit detectable by TEM. It was also confirmed that the optimization of the growth and design parameters allowed the growth of InAsSb bulk layers without any apparent self-ordering.[11]

In this work an unstrained and unrelaxed $InAs_{0.6}Sb_{0.4}$ 1-μm-thick bulk layer was gown by MBE on a 3 μm thick GaInSb compositionally graded buffer layer and a 500 nm $Ga_{0.66}In_{0.34}Sb$ virtual substrate.[8] We utilized this layer as the absorber section of the barrier photodetector. This nominally undoped alloy section demonstrated an absorption edge near 9.5 μm at 77 K. Figure 1(a) is a schematic band diagram of the barrier photodetector heterostructure under flat band condition. The InAsSb absorber was grown undoped. Our assumption about the n-type of InAsSb is based on its similarity to InAs. The background electron concentration in this layer cannot be high (probably below 10^{16} cm^{-3}) since we did not observe the Burstein-Moss shift between the detector cut-off wavelength (as shown in Figure 2(b)) and the low energy edge of the photoluminescence spectra of the absorber (see also Ref. 7). For the barrier layer we selected an $Al_{0.75}In_{0.25}Sb$ ternary alloy that was lattice matched to $InAs_{0.6}Sb_{0.4}$. The calculation predicted that the large band offset in conduction band between the InAsSb absorber and the AlInSb barrier should suppress the electron transport from the absorber to the n+ InAsSb contact layer. The valence band edges can be expected to be nearly aligned between InAsSb and AlInSb; hence, the photo and thermally generated holes can reach the top contact. This idealized picture neglects any effects of possible residual doping in the AlInSb.

To elucidate the effect of the doping type and density of the AlInSb barrier layer on the performance parameters of the barrier photodetectors we produced devices with different intentional doping levels. We compared nominally undoped, with moderately p-doped (Be, 10^{16} cm^{-3}), and heavily p-doped (Be, 10^{17} cm^{-3}) AlInSb. The wafers were processed into front side illuminated devices (Figure 1(b)). We used an inductively coupled $H_2/CH_4/Ar$ plasma reactive ion etching process to define the top contacts into square mesas with sides ranging from 50 to 600 μm. A silicon nitride mask was used for mesa definition, and the etching process was stopped in the top half of the barrier layer as confirmed by the Scanning Electron Microscopy (SEM) image shown in the inset of Figure 1(b). The mesas were covered by a 300-nm-thick silicon nitride layer followed by the deposition of Ti/Pt/Au contacts. Square optical windows with sides of 200, 300, and 400 μm were opened on the front side on mesas with side lengths of 400, 500, and 600 μm, respectively. The external quantum efficiency (EQE) was measured with illumination from the epi-side. No antireflection coating was applied. The backside contact consisted of an annealed Ni/Au/Ge/Ni/Au layer and a Ti/Pt/Au final metallization.

a)Electronic mail: gregory.belenky@stonybrook.edu

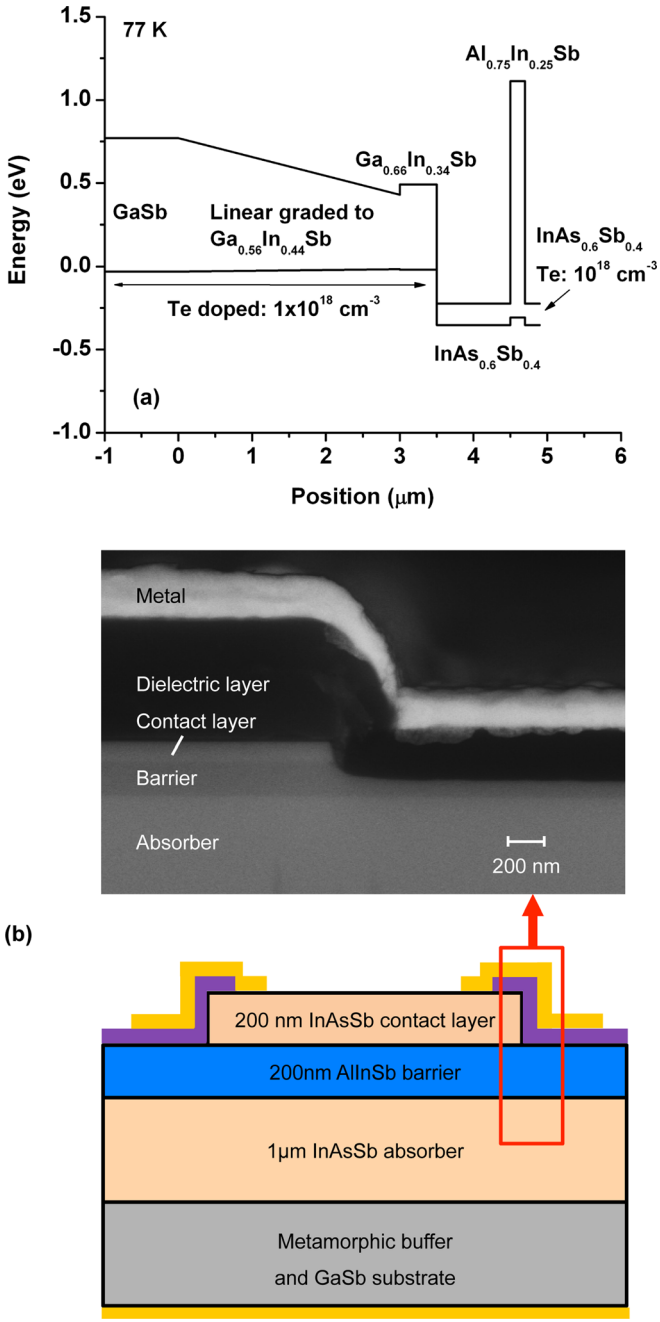

FIG. 1. (a) Schematic band diagram of the detector heterostructure with undoped InAsSb absorber under flat band condition. The 500 nm $Ga_{0.66}In_{0.34}Sb$ virtual substrate layer is lattice matched to the absorber (see Ref. 8). No bowing of the valence band offset was assumed. (b) Top: SEM image of the cleaved mesa cross-section; bottom: the schematic structure of the front side illuminated detectors.

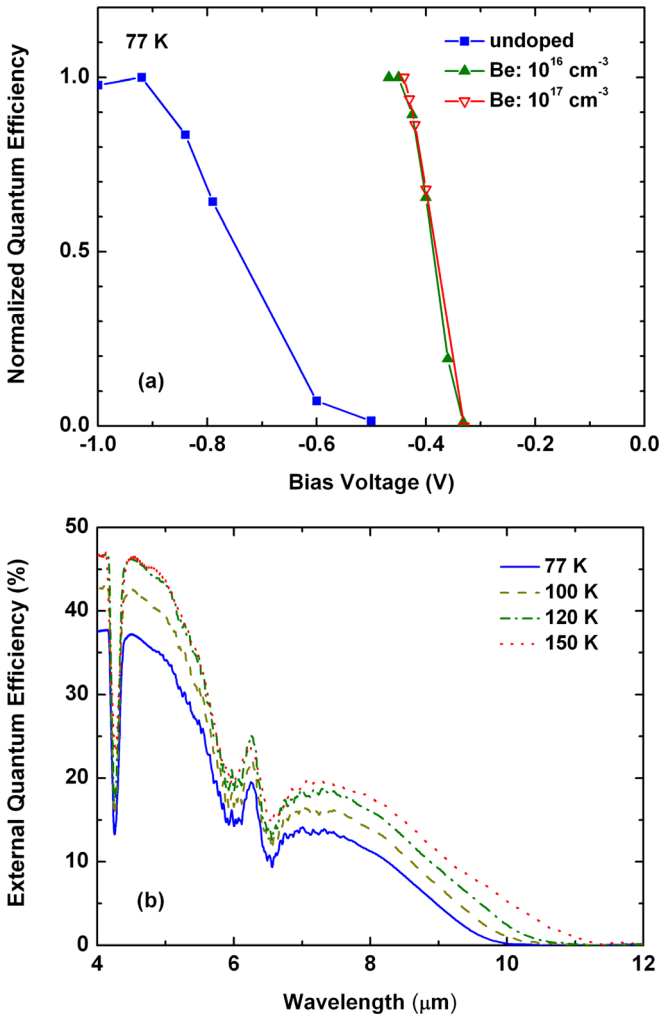

FIG. 2. (a) The bias dependence of normalized EQE at 8 μm at 77 K for all three types of devices. (b) EQE spectra at biases corresponding to saturation in a temperature range from 77 K to 150 K. The spectra were smoothed by averaging of adjacent points. The atmospheric absorption causes the distortions of the spectra within the 5–7 μm regions.

The quantum efficiency was measured using an 800 °C blackbody source with a 2.5 mm aperture at distances from 5 to 30 cm. Figure 2(a) plots the bias dependence of the EQE at 8 μm measured at 77 K for all three types of devices. A bias of 0.45 V was required for devices with moderately and heavily p-doped barriers to reach saturation of the EQE while a bias nearly double that was required for devices with nominally undoped barrier layers. Figure 2(b) plots the EQE spectrum at the bias corresponding to saturation. At 77 K more than 10% efficiency is demonstrated at 8 μm. When the device was heated up to 150 K, the bandgap was reduced, shifting the EQE spectrum correspondingly, and more than 10% of EQE was obtained near 9 μm.

For the structure with AlInSb layer grown undoped the potential profile of the valence band is formed by the band offset between InAsSb and AlInSb, by the contribution of the modulation doping effect (we assume slightly n-type AlInSb) and by the difference in doping of the absorber and the top contact layer. In this case the major portion of the bias voltage drops across the AlInSb layer, and a relatively large bias voltage (0.9 V) is required to enable the hole transport.

Apparently even low p-doping of the AlInSb layer leads to the annihilation of the effect of modulation doping and decreases the voltage drop across the AlInSb barrier. The potential barrier which impedes the hole transport in cases of structures with p-doped AlInSb is smaller which results in a moderate bias (0.45 V) and the identical behavior of dependences EQE versus V for both p-doped structures (Figure 2(a)).

The values of EQE in the 1-μm-thick absorber correspond to an estimated absorption coefficient above 2000 cm^{-1} for photon energies of about 15 meV above the absorption edge (e.g., at the wavelength of 8 μm at 77 K). The high

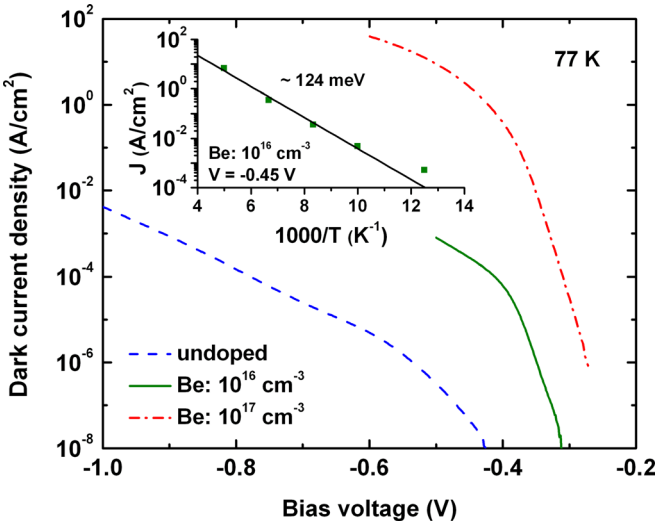

FIG. 3. Dark current density as a function of bias voltage for all three types of devices at 77 K. No dependence of dark current density on mesa size was observed. Inset: Temperature dependence of the dark current density at 0.45 V bias for the device with moderately doped barrier. The calculated activation energy from 100 K to 200 K is 124 meV.

absorption coefficient value is an inherent advantage of the bulk III–V absorber material.

Figure 3 plots the dark current-voltage characteristics at 77 K for all three types of devices. The dark current values corresponding to biases required to reach the maximum EQE are nearly the same for devices with nominally undoped and moderately p-doped barrier layers. The device with moderately doped barrier layer has a dark current density of 5×10^{-4} A/cm^2 at a bias voltage of 0.45 V. The estimated specific detectivity of this device at 77 K is about 4×10^{10} cm Hz$^{1/2}$ W^{-1}. The device with heavily p-doped barrier demonstrates much higher dark current values. The inset in Figure 3 plots the temperature dependence of the dark current density (bias is 0.45 V) for a device with a moderately doped barrier layer. In the temperature range above 100 K the activation energy for the dark current density at this bias voltage was equal to 124 meV.

The character of the I–V for structures with AlInSb layer grown undoped reflects the complex nature of the potential profile in the valence band discussed above. The suppression of the barrier for hole transport occurs gradually over a wide range of bias voltages. We can see the change of the slope at the bias voltage of 0.6 V where EQE starts; however, no signature is visible at 0.9 V where EQE reaches the maximum. At high voltage the contribution of G-R current increases, the activation energy of temperature-dependent dark current decreased from 124 meV at 0.6 V to 77 meV at 1 V bias. Taking into account the small energy gap of heterostructure materials the effect of tunneling can affect the I–V curve behavior (see the difference in the I–V for structures with different p-doping in Figure 3).

In summary, long-wave infrared nBn photodetectors with bulk, unrelaxed $InAs_{0.6}Sb_{0.4}$ absorbers and $Al_{0.75}In_{0.25}Sb$ barriers grown on compositionally graded GaInSb buffers on GaSb substrates were fabricated by molecular beam epitaxy and characterized. The heterostructures with 1-μm-thick absorbers demonstrated external quantum efficiencies of 12% and 18% at 8 μm at a bias voltage of 0.45 V and temperatures of T = 77 and 150 K, respectively. The estimated specific detectivity of this device at 77 K is about 4×10^{10} cm Hz$^{1/2}$ W^{-1}.

The work was supported by US Army Research Office through grants (Nos. W911NF1110109 and W911NF1220057) and by US National Science Foundation through grant (No. DMR1160843).

[1]S. Maimon and G. W. Wicks, Appl. Phys. Lett. **89**, 151109 (2006).
[2]P. Klipstein, Proc. SPIE **6940**, 69402U (2008).
[3]D. Z.-Y. Ting, C. J. Hill, A. Soibel, S. A. Keo, J. M. Mumolo, J. Nguyen, and S. D. Gunapala, Appl. Phys. Lett. **95**, 023508 (2009).
[4]B.-M. Nguyen, S. Bogdanov, S. A. Pour, and M. Razeghi, Appl. Phys. Lett. **95**, 183502 (2009).
[5]H. S. Kim, O. O. Cellek, Z.-Y. Lin, Z.-Y. He, X.-H. Zhao, S. Liu, H. Li, and Y.-H. Zhang, Appl. Phys. Lett. **101**, 161114 (2012).
[6]N. Gautam, S. Myers, A. V. Barve, B. Klein, E. P. Smith, D. R. Rhiger, H. S. Kim, Z.-B. Tian, and S. Krishna, IEEE J. Quantum Electron. **49**, 211 (2013).
[7]G. Belenky, D. Donetsky, G. Kipshidze, D. Wang, L. Shterengas, W. L. Sarney, and S. P. Svensson, Appl. Phys. Lett. **99**, 141116 (2011).
[8]G. Belenky, D. Wang, Y. Lin, D. Donetsky, G. Kipshidze, L. Shterengas, D. Westerfeld, W. L. Sarney, and S. P. Svensson, Appl. Phys. Lett. **102**, 111108 (2013).
[9]D. Wang, Y. Lin, D. Donetsky, G. Kipshidze, L. Shterengas, G. Belenky, S. P. Svensson, W. L. Sarney, and H. Hier, Proc. SPIE **8704**, 870410 (2013).
[10]G. Kipshidze, T. Hosoda, W. L. Sarney, L. Shterengas, and G. Belenky, IEEE Photon. Technol. Lett. **23**, 317 (2011).
[11]S. P. Svensson, W. L. Sarney, H. Hier, Y. Lin, D. Wang, D. Donetsky, L. Shterengas, G. Kipshidze, and G. Belenky, Phys. Rev. B **86**, 245205 (2012).